Characterisation of low-energy Compton Scattering

Lukas Kostal

***Abstract*—A theoretical model of Compton scattering is introduced and an experiment to measure angular dependance in the low-energy domain at $E_\gamma = 661.657(3)$ is described. A Monte Carlo simulation of the experiment is presented. The theoretical model is shown to agree with measured and simulated data with reduced chi squared values of $\chi_\nu^{2\ \text{data}} = 0.20$ and $\chi_\nu^{2\ \text{sim}} = 0.14$ for the energy of scattered photons and $\chi_\nu^{2\ \text{data}} = 0.94$ and $\chi_\nu^{2\ \text{sim}} = 2.1$ for the differential cross section. Sources of random and systematic errors are then discussed and used to motivate future improvements.**

I. Introduction

The main mechanisms by which gamma rays interact with matter are the photoelectric effect, Compton scattering and pair production. Of these, Compton scattering is significant over the greatest range of energies from keV up to GeV. As a result, it affects a wide range of systems such as scintillation detectors causing the Compton edge and limiting detector sensitivity. An accurate model of Compton scattering is therefore essential for designing nuclear and particle physics experiments.

II. Theory

A photon of initial energy E_γ incident on an e^- with rest mass m_e at a scattering angle θ is scattered with a final energy E'_γ given by

$$E'_\gamma = \frac{E_\gamma}{1 + \frac{E_\gamma}{m_e c^2}(1 + \cos\theta)} \tag{1}$$

A differential cross section (DCS) for Compton scattering is given by the Klein-Nishina formula [1] which can be derived by considering the transition probability of the lowest order interactions in QED [2] giving

$$\frac{d\sigma}{d\Omega} = \frac{1}{2} r_e^2 \left(\frac{E'_\gamma}{E_\gamma}\right)^2 \left(\frac{E'_\gamma}{E_\gamma} + \frac{E_\gamma}{E'_\gamma} - \sin^2\theta\right) \tag{2}$$

Where r_e is the classical electron radius.

The differential cross section can also be calculated from experimental data [3] as

$$\frac{d\sigma}{d\Omega} = \frac{I}{\phi \Omega N_e} \tag{3}$$

Where I is the rate of scattered photons, ϕ is the flux of photons incident on the scattering target, Ω is the solid angle of the detector from the scattering target and N_e is the number of electrons in the target available for scattering.

III. Experimental Setup

The experiment is setup as shown on Fig. 1 with a pure Al cylindrical target positioned in the center. A 50 mm thick Pb shielding block is positioned between the source and the detector to prevent detecting unscattered photons.

The source consists of a 1 mm dia. ^{137}Cs sphere with an approximate activity of $A \approx 3.3 \pm 0.1$ MBq. The ^{137}Cs undergoes β^- decay into metastable $^{137\mathrm{m}}$Ba which decays via emission of gamma ray photons at $E_\gamma = 661.657(3)$ keV. The source is encased in an Al body which is inserted into a Pb housing with a narrow aperture.

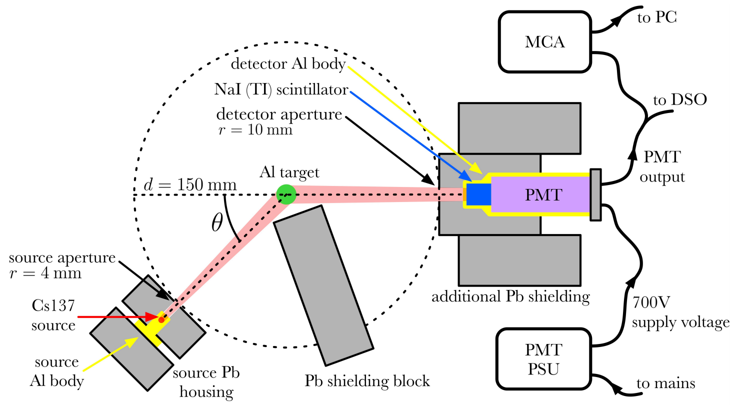

Fig. 1: Plan view of the experimental setup for scattering at an angle θ.

Scattered photons are detected using a Harshaw 6S8/2A scintillation detector which consists of a NaI(TI) crystal optically couplet to a photomultiplier tube (PMT) contained in a solid Al body with a 0.4 mm thick aperture [4]. The detector assembly is then inserted into a Pb housing with a small aperture which increases the angular resolution at the expense of the geometric efficiency of the detector.

The PMT is powered by a variable high voltage power supply (PSU) set to approx. $U = 700$ V chosen to provide the highest possible PMT gain. The output of the PMT is then connected to a multi channel analyser (MCA) with an integrated preamplifier stage with a variable gain g. The MCA is configured to operate in pulse height analysis mode [5] with 11 bit resolution. The MCA is connected to a PC running CASSY Lab 2 data acquisition program.

IV. Methodology

Measurements for energy calibration of the PMT detector are taken for 8 different sources with a total of 12 distinct peaks with energies ranging from $E_\gamma = 21.9906(2)$ keV for ^{109}Sr up to $E_\gamma = 1332.492(4)$ keV for ^{60}Co [6]. The measurement time is varied up to 1000 s depending on the activity of the source, and the preamplifier gain g is set to obtain the highest energy resolution for each source. A 2000 s background measurement is taken without a source.

The ^{137}Cs is inserted into the Pb housing positioned at a given scattering angle and aligned using a set square. A Python script is used to calculate the optimum gain g at a given θ. A measurement is then taken over 1000 s. The scattering target is then removed and a no-target measurement is taken with the same settings. The data is exported from CASSY Lab 2 in the form of .csv files. Measurements are repeated for scattering angles from 0° up to 140° in increments of 10°.

To measure the effective activity of the ^{137}Sc source including the peak detector efficiency ε the source is placed at the center of the setup and a 600 s measurement is taken.

Additionally, the geometry of the entire setup as well as the mass of the target m are measured.

V. Simulation

A Monte Carlo simulation of the experiment is written using the GEANT4 toolkit [7]. The simulation includes the entire experimental setup geometry excluding the PMT as shown in the Appendix. The source is simulated as an Al body within which photons of a specific energy are emitted isotropically. The detector is simulated as a $\mathrm{NaI(TI)}$ crystal encased in the Al body of the detector. Custom messenger commands are used to reproduce the experimental method written in the form of a macro file. Information about particles incident on the detector such as total energy and momentum direction vector are written into a ROOT file [8].

The simulation is ran in multithreaded mode with 2×10^8 photons simulated at each scattering angle.

A Python script is used to load the ROOT files and histogram the data which is then written into a .csv file.

VI. Data Analysis

All of the simulation source files, analysis scripts as well as measured and simulated data can be found in the GitHub Repository [9] of the experiment.

Throughout the analysis all uncertainties in the number of counts per bin are taken to be the error from Poisson counting statistics. Uncertainties on all fitting parameters are calculated from the covariance matrix. Uncertainty on the scattering angle is determined from the geometry of the setup.

The calibration data is loaded, adjusted for the gain g, the background is resampled and subtracted. Peaks in the spectra are automatically matched to specified reference peaks with energies taken from the IAEA Vol. 1 database [6] and fitted with a Gaussian. A polynomial is then fitted onto the calibration datapoints using orthogonal distance regression (ODR) [10] and a reduced chi squared (RCS) test is performed.

Data from the scattering measurements is loaded and the no-target measurements are subtracted. The channel number is adjusted for the gain g and converted to energy using the calibration polynomial. A preliminary Gaussian fit is performed over the entire spectrum with parameters restricted to $\pm 20\%$ of the theoretical prediction. A second unrestricted Gaussian fit is then performed over points within ± 1 full width at halve maximum (FWHM) of the preliminary fit.

The mean of the Gaussian represents the energy E'_γ and a RCS test is performed against the theoretical model from (1).

The rate of scattered photons I is calculated as the area of the Gaussian peak divided by the measurement time. A similar analysis is also performed on the source activity measurements to determine the effective activity of the $^{237}\mathrm{Cs}$ source $A' = A\varepsilon$ which is used to calculate the flux ϕ of photons incident on the scattering target. The DCS is calculated using (3) and a RCS test is performed against the Klein-Nishina model (2).

VII. Results

A 3rd order calibration is performed giving a RCS value of $\chi^{2\ cal}_{\nu} = 0.085\ \mathrm{(2sf)}$ and higher order residuals which are 0 to within the expected uncertainty.

The effective activity of the source is measured to be $A' = 2.38 \pm 0.48\ \mathrm{MBq}$ corresponding to an approximate detector efficiency of $\varepsilon \approx 71 \pm 14\ \%$.

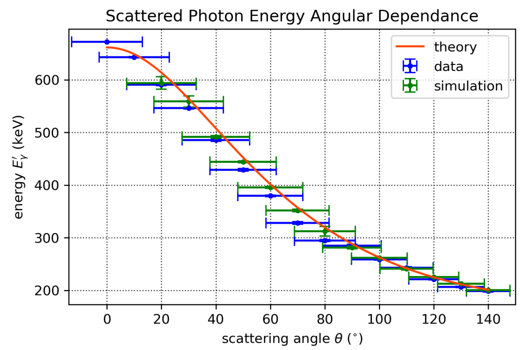

Fig. 2: Energy of scattered photons E'_γ agains the scattering angle θ.

From Fig. 2 it can be seen that both the measured and simulated energy of scattered photons agrees with the theoretical curve to within the expected uncertainty with RCS values of $\chi^{2\ \mathrm{data}}_{\nu} = 0.20\ \mathrm{(2sf)}$ and $\chi^{2\ \mathrm{sim}}_{\nu} = 0.14\ \mathrm{(2sf)}$.

The dominant uncertainty is on the scattering angle θ caused by the extended (non-point-like) source, target and detector. As indicated by the low RCS value, the geometric calculation of this uncertainty is an overestimate as it assumes a uniform angular distribution of the scattered photons.

All points except $\theta = 0°$ lie below the theoretical curve. This is explained by a systematic effect caused by Compton scattering within the Al body of the source and the detector which causes the peaks to become left-skewed.

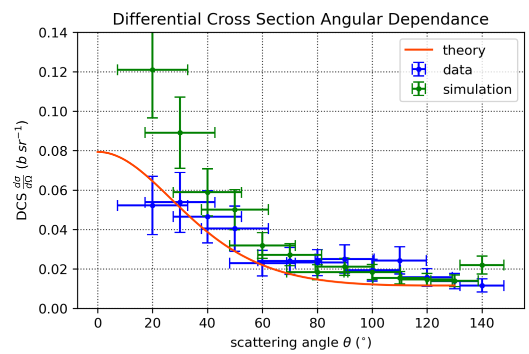

Fig. 3: Calculated differential cross section against the scattering angle θ.

From Fig. 3 it can be seen that the DCS calculated from both the measured and simulated data follows the Klein-Nishina formula with RCS values of $\chi^{2\ \mathrm{data}}_{\nu} = 0.94\ \mathrm{(2sf)}$ and $\chi^{2\ \mathrm{sim}}_{\nu} = 2.1\ \mathrm{(2sf)}$ respectively.

The high calculated DCS from simulated data at low θ is likely caused by photons passing through a narrow gap between the scattering target and the Pb shielding block.

The rate of scattered photons I depends on the peak detector efficiency ε which is assumed to be constant. In reality it varies with the energy of the photons being detected and therefore with θ giving rise to a systematic error.

VIII. Conclusion

The angular dependance from the theoretical model can be concluded to be in agreement with the presented experiment and simulation to within the expected uncertainty with RCS values ranging from $\chi^2_\nu = 2.1\ \mathrm{(2sf)}$ down to $\chi^2_\nu = 0.14\ \mathrm{(2sf)}$.

In future experiments the angular resolution can be improved by using a narrower target and a smaller detector aperture. Measurements for $\theta < 0°$ can be taken to check for systematic errors due to any asymmetries in the setup.

References

[1] C.-K. Qiao, J.-W. Wei, and L. Chen, "An overview of the compton scattering calculation," *Crystals*, vol. 11, no. 5, p. 525, 2021.

[2] D. Millar, "A calculation of the differential cross section for compton scattering in tree-level quantum electrodynamics," *Lecture notes*, p. 25, 2014.

[3] A. C. Melissinos and J. Napolitano, *Experiments in modern physics*. Gulf Professional Publishing, 2003.

[4] L. D. GmbH, "Scintillation counter (559 901)," [Online]. Available: https://www.leybold-shop.com/catalog/product/view/id/3291/s/scintillation-counter-559901/category/2036/, 1999.

[5] E. R. Thuraka, R. Ganesh, D. B. Prakash, P. Sreekanth, P. R. Reddy, and M. Likhita, "Digital multi-channel analyzer for detection and analysis of radiation in nuclear spectroscopy," *Materials Today: Proceedings*, vol. 38, pp. 3160–3167, 2021.

[6] O. Helene, V. R. Vanin, R. G. Helmer, E. Schönfeld, R. Dersch, C. M. Baglin, E. Browne, R. M. Castro, and P. R. Pascholati, "Update of x-ray and gamma-ray decay data standards for detector calibration and other applications," *International Atomic Energy Agency: Vienna*, vol. 210, 2007.

[7] S. Agostinelli, J. Allison, K. a. Amako, J. Apostolakis, H. Araujo, P. Arce, M. Asai, D. Axen, S. Banerjee, G. Barrand *et al.*, "Geant4-a simulation toolkit," *Nuclear instruments and methods in physics research section A: Accelerators, Spectrometers, Detectors and Associated Equipment*, vol. 506, no. 3, pp. 250–303, 2003.

[8] R. Brun and F. Rademakers, "Root-an object oriented data analysis framework," *Nuclear instruments and methods in physics research section A: accelerators, spectrometers, detectors and associated equipment*, vol. 389, no. 1-2, pp. 81–86, 1997.

[9] L. Kostal, "Caracterisation of low-energy Compton Scattering GitHub repository," [Online]. Available: https://github.com/KostalLukas/Characterisation-of-Low-Energy-Compton-Scattering, 2023.

[10] P. T. Boggs, P. T. Boggs, J. E. Rogers, and R. B. Schnabel, "User's reference guide for odrpack version 2.01: Software for weighted orthogonal distance regression," 1992.

Appendix

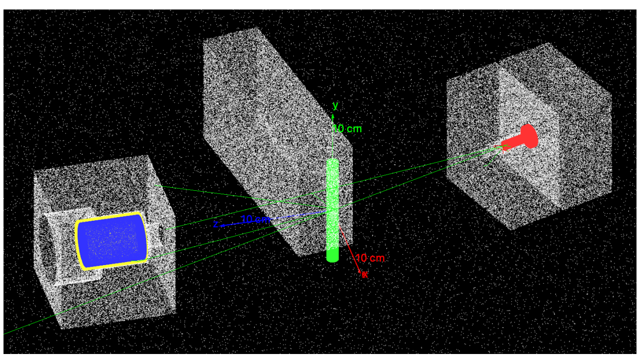

Fig. 4: Visualisation of simulated experimental setup in GEANT4 with source at $\theta = 20°$. The Al source body in red, scattering target in green, $\mathrm{NaI(TI)}$ scintillator in blue and Al scintillator body in yellow.

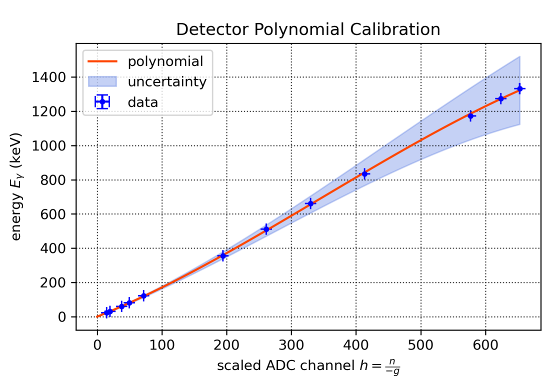

Fig. 5: Detector calibration curve using a 3rd order polynomial. Each point corresponds to one of the 12 reference peaks used for the calibration.

Cycle 1 Feedback

The presentation was polished and well thought out with clear explanations and delivery. Introductory slides provided detailed background theory with evidence of further reading, and content demonstrating good initiative and strong technical ability. Excellent use of diagrams and graphs were correctly formatted with labelled axes and data. Very impressive attempt to match theory and experiment for thermal energy distribution. Some slides contained excessive amount of bullet points with dense text amount of text. Instead, for short presentations such as this, use bullet points to highlight only the key talking point - you can then elaborate on these orally. Contents on slide 1 was flashed up but never mentioned.